ARL-TR-8115 ● AUG 2017

US Army Research Laboratory

Multiflash X-ray with Image Detanglement for Single Image Isolation

by Willard Casey Uhlig

NOTICES

Disclaimers

The findings in this report are not to be construed as an official Department of the Army position unless so designated by other authorized documents.

Citation of manufacturer's or trade names does not constitute an official endorsement or approval of the use thereof.

Destroy this report when it is no longer needed. Do not return it to the originator.

ARL-TR-8115 ● AUG 2017

US Army Research Laboratory

Multiflash X-ray with Image Detanglement for Single Image Isolation

by Willard Casey Uhlig
Weapons and Materials Research Directorate, ARL

REPORT DOCUMENTATION PAGE

Form Approved
OMB No. 0704-0188

1. REPORT DATE *(DD-MM-YYYY)*	2. REPORT TYPE	3. DATES COVERED (From - To)
August 2017	Technical Report	January 2016–March 2017

4. TITLE AND SUBTITLE
Multiflash X-ray with Image Detanglement for Single Image Isolation

5a. CONTRACT NUMBER

5b. GRANT NUMBER

5c. PROGRAM ELEMENT NUMBER

6. AUTHOR(S)
Willard Casey Uhlig

5d. PROJECT NUMBER

5e. TASK NUMBER

5f. WORK UNIT NUMBER

7. PERFORMING ORGANIZATION NAME(S) AND ADDRESS(ES)
US Army Research Laboratory
Weapons and Materials Research Directorate
ATTN: RDRL-WMP-A
Aberdeen Proving Ground, MD 21005

8. PERFORMING ORGANIZATION REPORT NUMBER
ARL-TR-8115

9. SPONSORING/MONITORING AGENCY NAME(S) AND ADDRESS(ES)

10. SPONSOR/MONITOR'S ACRONYM(S)

11. SPONSOR/MONITOR'S REPORT NUMBER(S)

12. DISTRIBUTION/AVAILABILITY STATEMENT
Approved for public release; distribution is unlimited.

13. SUPPLEMENTARY NOTES

14. ABSTRACT
A new capability was conceived and developed to capture multiple flash X-rays on a single film or phosphor screen and digitally detangle the resulting image into separate images for each individual flash. This is accomplished via the use of multiple flash X-ray heads geometrically placed with respect to a shadow mask in close proximity to the detection screen. The small holes in the shadow mask only allow X-rays from each head to pass through along a unique trajectory to specific pixels of the screen based on the placement of the head, mask, and screen. Thus, the location of the pixels associated with each flash are known and separated into individual images. A proof-of-principle study was performed using 4 X-ray flashes and copper masks with sub-millimeter holes that allowed development of the required image-analysis algorithms. While using the method with 4 flashes decreased the image resolution by half and reduced the number of photons striking the phosphor screen to one-quarter, 4 images were successfully detangled without any flash-to-flash overlap in the images.

15. SUBJECT TERMS
flash X-ray, ballistic diagnostics, shadow mask, radiographic diagnostics, multiple flash X-ray imaging

16. SECURITY CLASSIFICATION OF:			17. LIMITATION OF ABSTRACT	18. NUMBER OF PAGES	19a. NAME OF RESPONSIBLE PERSON
a. REPORT	b. ABSTRACT	c. THIS PAGE			Willard Casey Uhlig
Unclassified	Unclassified	Unclassified	UU	22	19b. TELEPHONE NUMBER (Include area code) 410-278-3997

Contents

List of Figures iv

Acknowledgments v

1. Introduction 1

2. Conceptual Outline 2

2.1 Geometric Configuration 2

2.2 Image-Analysis Algorithm 4

2.3 Calculation on a Test Image 6

3. Experimental Proof of Concept 7

3.1 Copper Mask One: 0.6 mm Thick, 1.0-mm Holes 8

3.2 Copper Mask Two: 1.8 mm Thick, 0.79-mm Holes 9

3.3 Future: Laser-Drilled Tungsten Mask 9

4. Conclusion 11

5. References 12

List of Symbols, Acronyms, and Abbreviations 13

Distribution List 14

List of Figures

Fig. 1 Illustration of the electron beam lines for a cathode ray tube color television 1

Fig. 2 Illustration of square grid shadow mask 3

Fig. 3 Geometric configuration of the shadow mask concept, showing 2-D ray tracing of 2 of the 4 X-ray heads. The shadowed box at the bottom of the figure shows the front view of the placement of the 4 X-ray heads. 4

Fig. 4 Example of generating a new pixel from a region-of-interest from the original radiograph 5

Fig. 5 Test image to determine effectiveness of image-analysis algorithm 7

Fig. 6 a) Resulting images from the third “flash” using the algorithm on a test image with a multiple pixel object where the averaged sample area was too large and b) a reduced sample area 7

Fig. 7 Radiographs from a thin copper shadow mask with 2.15-mm-hole spacing 8

Fig. 8 Four flash radiograph of a 30-cal. bullet in 4 different positions with a 1.8-mm-copper shadow mask with 1.8-mm-hole spacing and the associated detangled images 9

Fig. 9 X-ray photon attenuation of tungsten and tantalum sheets of 380- and 245-μm thicknesses 10

Fig. 10 Proposed shadow mask design for 0.38-mm-thick tungsten sheet for X-ray image detanglement with 0.5-mm resolution 11

Acknowledgments

The author would like to thank Dr Charles Hummer for the inspiration of this concept. Also, thanks is given to Mr Keith Mahan and Mr Steven Davis for their efforts in machining some of the shadow masks.

INTENTIONALLY LEFT BLANK.

1. Introduction

In the 1940s and early 50s, RCA made the color television a reality by developing a 3-electron gun and shadow mask combination, which ingeniously enabled separate illumination of red, green, and blue pixels.[1] An illustration of the electron beam lines and shadow mask concept, as well as an image of an original RCA color television tube, is shown in Fig. 1. A nice overview of the development and design of the scheme is presented in a 1963 *Popular Science* article.[2] For decades, that basic concept dominated the color television market. Those were the days when a large color television could fill up an entire room.

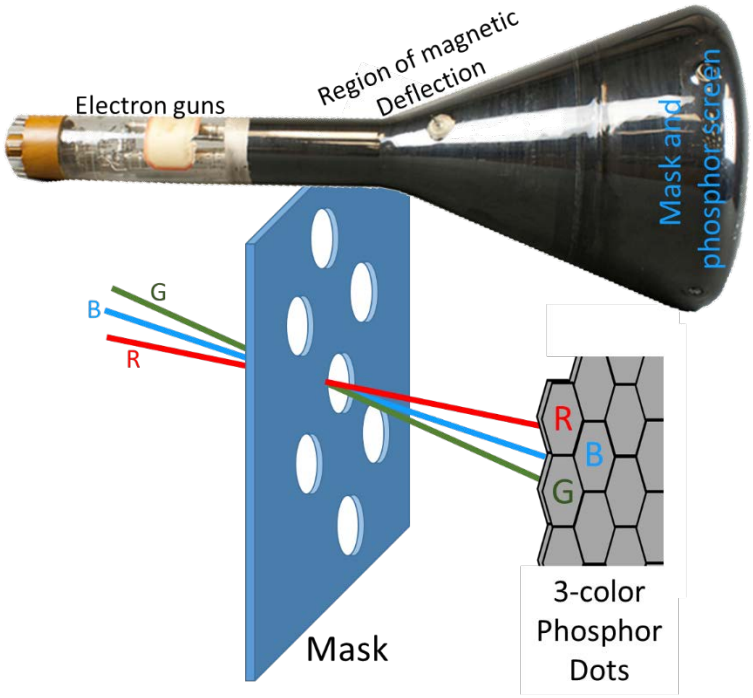

Fig. 1 Illustration of the electron beam lines for a cathode ray tube color television

In a similar vein, a new capability was conceived and developed to capture multiple flash X-rays on a single film or phosphor screen and digitally detangle the resulting image into separate images for each individual flash. Traditionally, multiple flash X-rays onto a single film have been used in ballistic and other high-speed events, with X-ray sources separated over a sufficient distance in an attempt to minimize overlap of the multiple flashes. However, in even relatively simple experiments the X-ray overlap can become difficult to decipher and obtain clear characterization of the event. The new capability presented here seeks to eliminate that complexity. This is accomplished via the use of multiple flash X-ray heads geometrically placed

with respect to a shadow mask, which is in close proximity to the detection screen. The small holes in the shadow mask only allow the X-rays from each head to pass along a unique trajectory to specific pixels of the film/phosphor screen based on the placement of the head, mask, and screen. Thus, the location of the pixels associated with each flash are known and separated into individual images.

A proof-of-principle study was performed using 4 X-ray flashes and copper masks with sub-millimeter holes that allowed development of the required image-analysis algorithms. While using the method with 4 flashes decreased the image resolution by half and reduced the number of photons striking the phosphor screen to one-quarter, 4 images were successfully detangled without any flash-to-flash overlap in the images.

2. Conceptual Outline

The use of 4 X-ray flashes results in a simple square grid shadow mask requirement. While the geometric location of the exposed screen is known, it must be correlated with the appropriate pixels of the resulting digital image as well as any pixels that may only be partially exposed and any uncertainties in the physical ability to precisely establish the experimental configuration.

2.1 Geometric Configuration

The most simple and direct way to align 4 X-ray tubes is to place the 4 tubes at the corners of a square, aligned with a square grid shadow mask. An illustration of such a shadow mask with square holes of width (w) and hole-to-hole spacing (b) is shown in Fig. 2. If the distance (d) from the X-ray source to the mask is much greater than the distance (s) between the shadow mask and the screen, then the width (P) of the exposed area on the screen is approximately equal to w. Thus, the hole-to-hole spacing can simply be set as twice the hole width. In Fig. 2, a box with dashed outlines shows the area of the screen (behind the mask) that would be exposed by the 4 flashes (labelled 1–4) through one of the holes as aligned directly with the first source for such a configuration. In reality w would be made slightly smaller than half b to avoid any overlap. (Section 2.2 will show how this can also be accomplished digitally by discarding boarder pixels if there is sufficient resolution in the original X-ray image.)

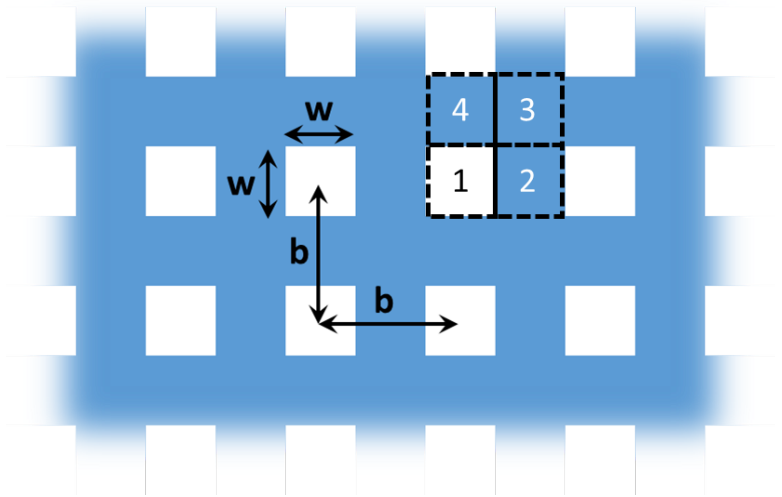

Fig. 2 Illustration of square grid shadow mask

Using this mask geometry, the distance from the center line on the screen (i.e., the location of exposure for a given hole and X-ray source) will be

$$F = \frac{(s+d)}{d}(m \pm H) \mp H\,, \tag{1}$$

where m is the distance from the center line to the hole location on the mask and H is the distance from the center line to the X-ray source as shown in Fig. 3, which gives a 2-D view of the shadow mask concept. The ± is determined by the position of the source with respect to the center line. The exposed area for a given hole/source pair (from which the intensity will be extracted for the new pixel of the processed image) will have a width of

$$P = \frac{2Hs}{d} = w\frac{(s+d)}{d}. \tag{2}$$

In full dimension, there will be an F_x and F_y for each corresponding m_x and m_y on the mask.

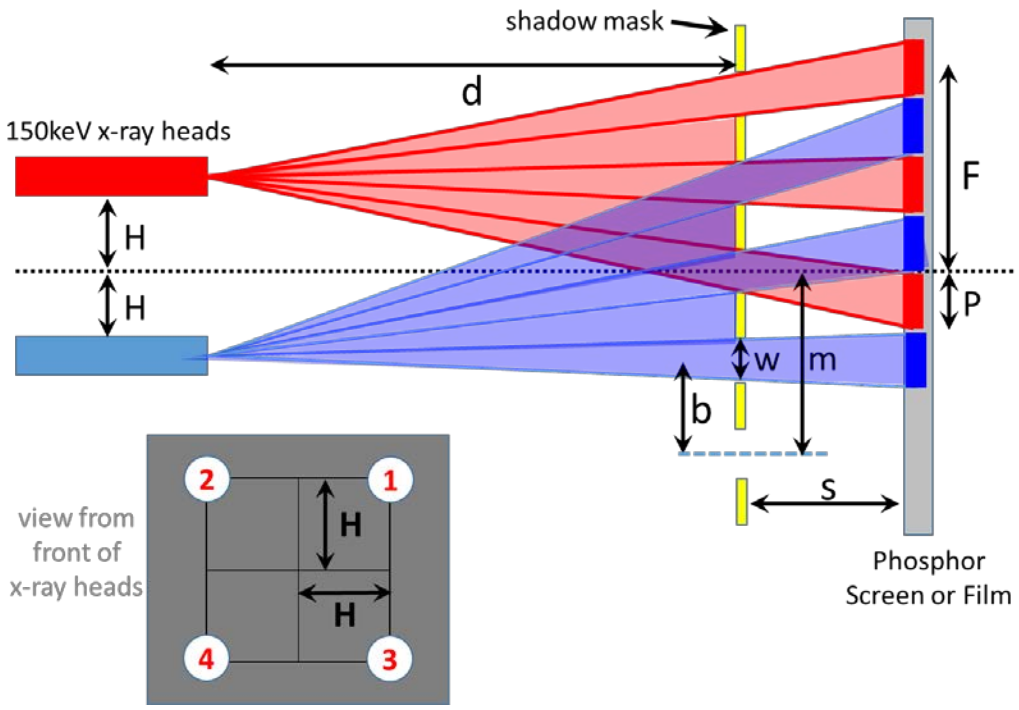

Fig. 3 Geometric configuration of the shadow mask concept, showing 2-D ray tracing of 2 of the 4 X-ray heads. The shadowed box at the bottom of the figure shows the front view of the placement of the 4 X-ray heads.

2.2 Image-Analysis Algorithm

There are 2 core objectives in developing the image-analysis algorithm: 1) the physical location of the exposed region, which will become a pixel in the new image (referred to as image1, image2, image3, or image4, corresponding to the X-ray flash of interest), needs to be determined in terms of pixel locations on the original digital radiograph (ORAD); and 2) an appropriate averaging of the value of the pixels within the exposed region-of-interest on the ORAD needs to be calculated. To find the location from the center line of the new pixel for the *n*th hole of the shadow mask use

$$m_x = \frac{1-N_x}{2}\, b + n_x b \quad \text{and} \quad m_y = \frac{1-N_y}{2}\, b + n_y b\,, \tag{3}$$

where N is the total number of pixels to be analyzed along an axis and is odd. This is relating to the (0,0) pixel's location in the top-left corner of the image. Using these values of m, F_x, and F_y as calculated in Eq. 1 would yield the center of the new image pixel. In obtaining the value for the new pixel, the average of the ORAD pixels completely encompassed within the region-of-interest and a weighted average of the partially covered pixels will be included.

Two separate scenarios are possible for averaging over the region-of-interest. If P is greater than twice the ORAD pixel width p_o, then it is guaranteed that at least one full pixel will be covered. In this case the average of the center pixels (i.e., fully covered) will be combined with the average of the pixels at each edge multiplied by the fraction of the pixel exposed by the region-of-interest correlating to the new image pixel. The pixels at the corners will be discarded for convenience. This can be observed in the example shown in Fig. 4, where the fully exposed pixels are shaded dark grey and the partially exposed pixels are shaded with slanted stripes. If overlap occurs from the other flash X-rays due to imprecise physical alignment of the mask and sources, the region-of-interest can be decreased digitally, encompassing fewer pixels. In the illusory example in Fig. 4, the center line is determined to be at the pixel position (242.77,195.85) on the ORAD. If N_x = 43, N_y = 33, d = 2000 mm, s = 43.5 mm, H = 25 mm, b = 2.15 mm, P = 0.92 mm (~ 15% reduction from b/2), and p_o = 0.254 mm, then the new (0,0) pixel of image1 would be centered at (63.29, 55.33) on the ORAD with F_x = –45.59 mm and F_y = –35.69 mm. The fraction at the top edge would be 0.49, the bottom edge 0.15, the left edge 0.53, and the right edge 0.11, for weighting the pixels in row 53, row 57, column 61, and column 65, respectively. This would be repeated for each new pixel location in both the x and y directions.

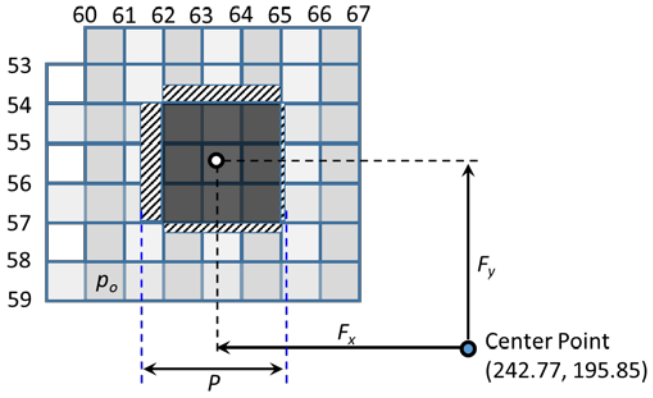

Fig. 4 Example of generating a new pixel from a region-of-interest from the original radiograph

While averaging is not necessary where multiple pixels are encompassed (i.e., just the center pixel could be chosen), there is no reason to discard data that could enhance the image. On the other hand, if $P < 2p_o$ the situation arises where it is possible that no original pixels are completely encompassed by the region-of-interest and averaging of the fractional pixels is necessary. Cazamias[3] generated an algorithm to calculate on a square mesh the area of overlap for individual elements with a square box. This method was adopted for the $P < 2p_o$ case. Again, each partially covered pixel (including corner pixels) was combined in a weighted

average to determine the value of the new image pixel. Because of the limited number of pixels within a region-of-interest, digital correction for overlap is not possible in this situation and requires physical compensation on the mask (i.e., reducing w to less than $b/2$). Ideally, configuring the X-ray set up with $P > 2p_o$ allows greater flexibility in eliminating overlap and possible influence of neighboring pixels than the $P < 2p_o$ case.

2.3 Calculation on a Test Image

To test the image-manipulation algorithms, an image with 4 bright pixels (representing an object moving in time and flashed with 4 pulsed X-ray sources) and a region of gradual brightness increase in the bottom-right corner (representing a stationary object) was created. The single bright pixels were placed in locations that would correspond to 4 different alignments through a mask and should be isolated on individual images after running the algorithm, while each image should include the gradual brightness increase in the corner. The left side of Fig. 5 shows the original image with a blue box outlining the region of the image used in the algorithm. The right side of Fig. 5 shows the 4 newly generated images. Each new image shows the bright bottom-right corner, but only 1 bright spot correlating to the moving object. For the test, $P = 3.23\ p_o$, thus the algorithm averaged over an approximate 3 × 3 block of pixels, and the 4 resulting images have a resolution 6.5 times lower than the original image (from $b \sim 2P$). Because the averaging covered 9 pixels and only 1 pixel was bright in the original area, the relative intensity between the moving object (bright pixel) and stationary object (corner region) has decreased. This is only a concern for real applications if the object to be radiographed is smaller than P. However, in practice, the object should be several times larger than the eventual pixel size of the new image, $F_n - F_{n-1}$ or $\sim 2P$.

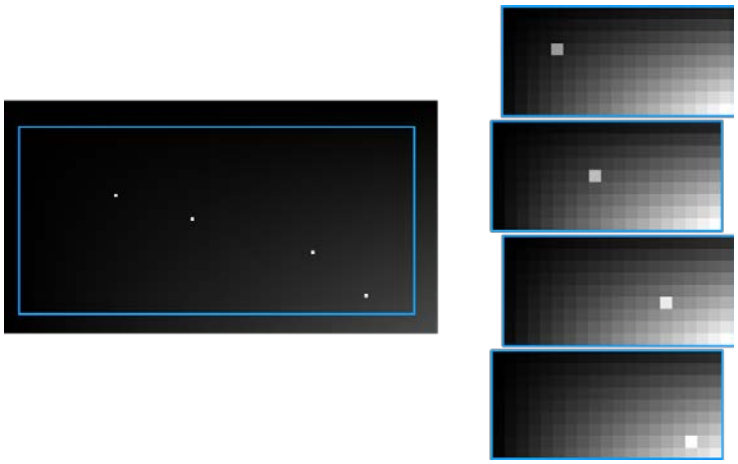

Fig. 5 Test image to determine effectiveness of image-analysis algorithm

If multiple pixels for the object are used or if the bright pixel is placed at the edge of the averaged area, overlap of the images can be replicated. Reducing *P* in the algorithm can reverse the effect as shown in Fig. 6, where a multiple pixel object having the same layout as Fig. 5 had too large of a sample area *P* (Fig. 6a) and a reduced sample area (Fig. 6b). The images should only show the results of the third "flash"; however, the larger sample area used in Fig. 6a allowed bleed-through of the first "flash". Narrowing the averaging area completely removes the overlap in Fig. 6b.

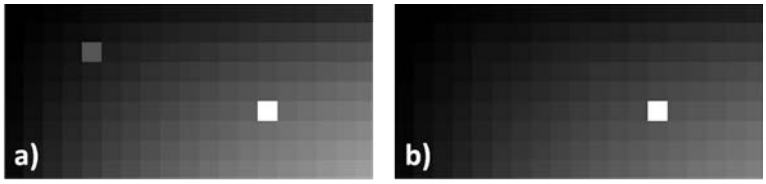

Fig. 6 a) Resulting images from the third "flash" using the algorithm on a test image with a multiple pixel object where the averaged sample area was too large and b) a reduced sample area

3. Experimental Proof of Concept

The factors effecting experimental implementation of this method include precise alignment of the system as well as the design and manufacture of the shadow mask. The mask must be opaque to the photons of the X-ray source. This is dependent on the photon energy, mask thickness, and mask material. While significant resolution is readily available for optical masks, thicker masks required to attenuate X-rays sufficiently is a much different requirement that is not readily available off-the-shelf. There also exists a limit in the ratio of the hole-width, the mask thickness, and the coverage area of the X-ray film or screen. If the material thickness is too

large compared to other critical geometries within the setup, significant shadowing will occur at the edges of the image. (Additionally, manufacturing deep holes whilst maintaining precise hole-size and shape becomes untenable.) Thus, the method will be limited to lower energy X-rays such as 150-kV flash X-ray tubes. With all these considerations in mind, a couple of masks made of copper with hole-sizes on the order of 1 mm (final image resolution order of 2 mm) were made to test the method. Then, a third mask was designed out of tungsten with 220-μm holes (final image resolution 0.5 mm) to test a realistic or usable system.

3.1 Copper Mask One: 0.6 mm Thick, 1.0-mm Holes

A 0.6-mm-thick copper shadow mask (mask1) with w = 1.0 mm and b = 2.15 mm was made as an initial test of the X-ray detanglement concept. A 150-kV flash X-ray was taken of a 30 cal. bullet and a 22-mm-wide washer with s = 44 mm, d = 2000 mm, and H = 25 mm. The bullet was moved approximately 12 mm to the right and a second flash X-ray was pulsed from position 2 (as outlined in Fig. 3). The mask was not precisely machined and the holes drilled (round) as can be seen in Fig. 7. Thus, P was reduced to 0.93 mm for the algorithm calculations.

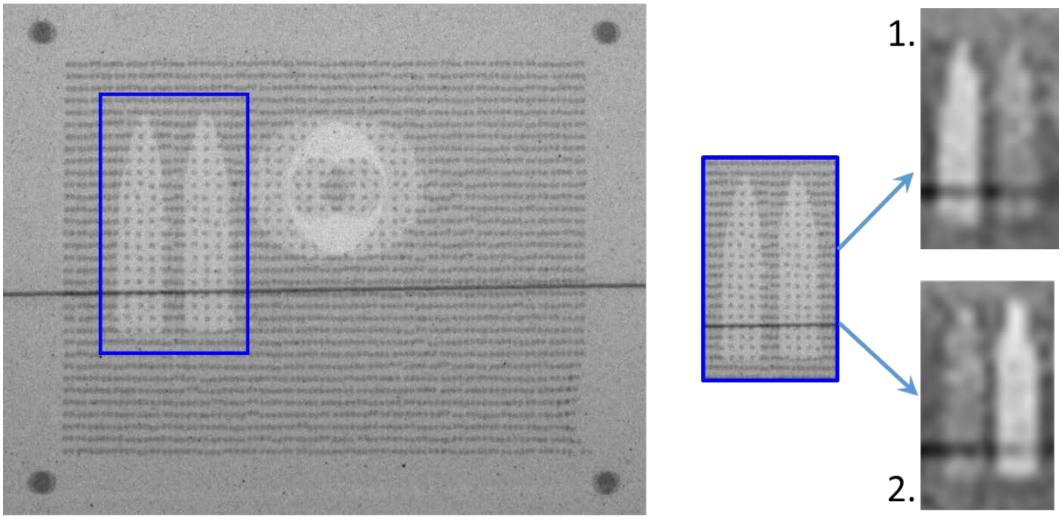

Fig. 7 Radiographs from a thin copper shadow mask with 2.15-mm-hole spacing

Shadows from exposure through the holes of the mask are visible in Fig. 7 and appear as horizontal lines of dots due to the overlap of the 2 X-rays. (If all 4 X-rays were flashed, dots would fill in the spacing between the lines as well.) The algorithm was applied to the region where the bullet appears in the radiograph highlighted in the blue box (Fig. 7). Image1 and image2 from the detanglement are labeled as 1 and 2. Obviously, 2.15 mm resolution on a 30 cal. bullet is not ideal, but the concept is clearly demonstrated. Additionally, shadowing from the alternate

X-ray flashes are visible in the detangled images (i.e., the bullet from flash 1 is lightly visible in image2 and vice-versa). The imprecise machine most likely contributes to the shadowing, but the largest contribution is the thickness of the copper. The copper does not attenuate the X-rays sufficiently.

3.2 Copper Mask Two: 1.8 mm Thick, 0.79-mm Holes

A second copper mask was machined with a smaller drill (0.79 mm) for slightly better resolution and an increased thickness (1.8 mm) for greater X-ray attenuation. While greater precision of hole location was implemented, unfortunately, multiple drill bits broke during construction causing missing pixels in the mask. However, excellent elimination of shadowing from flash-to-flash was achieved. Four 150-kV-flash X-rays were taken of a 30 cal. bullet in 4 different positions with a configuration of b = 1.8 mm, s = 40 mm, d = 2000 mm, and H = 22.5 mm. For the calculations P was set to 0.7 mm. The results are shown in Fig. 8. The black outlined box shows the region of the copper that was machined with the holes and thus used in the detanglement calculations. Despite the missing pixels, 4 separate radiographs are obtained clearly showing the position of the bullet as a function of time with very minimal shadowing.

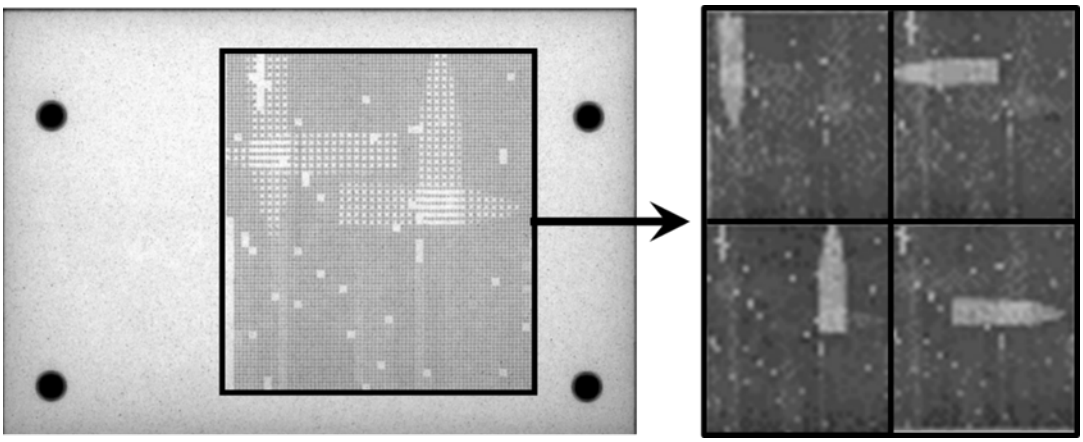

Fig. 8 Four flash radiograph of a 30-cal. bullet in 4 different positions with a 1.8-mm-copper shadow mask with 1.8-mm-hole spacing and the associated detangled images

3.3 Future: Laser-Drilled Tungsten Mask

Ideally a material would be used that is much better than copper at attenuating the X-rays. Gold has potential, but it is expensive and not very durable. Therefore, tungsten and tantalum were investigated. The data in Fig. 9 was generated using the X-ray attenuation coefficients available in the National Institute of Science and Technology (NIST) X-ray Mass Attenuation Coefficients Database.[4] The intensity

ratio is the photon intensity that passes through the material versus the initial intensity

$$\frac{I}{I_o} = e^{-\mu t}, \tag{4}$$

where μ is the X-ray mass attenuation coefficient and t is the thickness of the material. Minimizing this ratio will minimize shadowing between the detangled images. The energy profile of a 150-kV-flash X-ray pulse peaks between 60 and 90 kV. Thus, it is most important to focus in that region. Ironically, the attenuation shown in Fig. 9 shows a peak right in the middle of that region. Tungsten is a slightly better performer than tantalum and it is less expensive, so it was determined to use a 0.38-mm-thick tungsten sheet as a mask. Because sub-millimeter resolution is desired for the X-rays, precision laser drilling is the best hope for a mask of this material. A mask was designed with 0.22-mm-square holes with 0.5-mm hole-to-hole spacing and a total area of 76 × 76 mm^2, as shown in Fig. 10. Once this method of manufacture and appropriate attenuation is confirmed, a larger mask for use in dynamic experiments will be acquired.

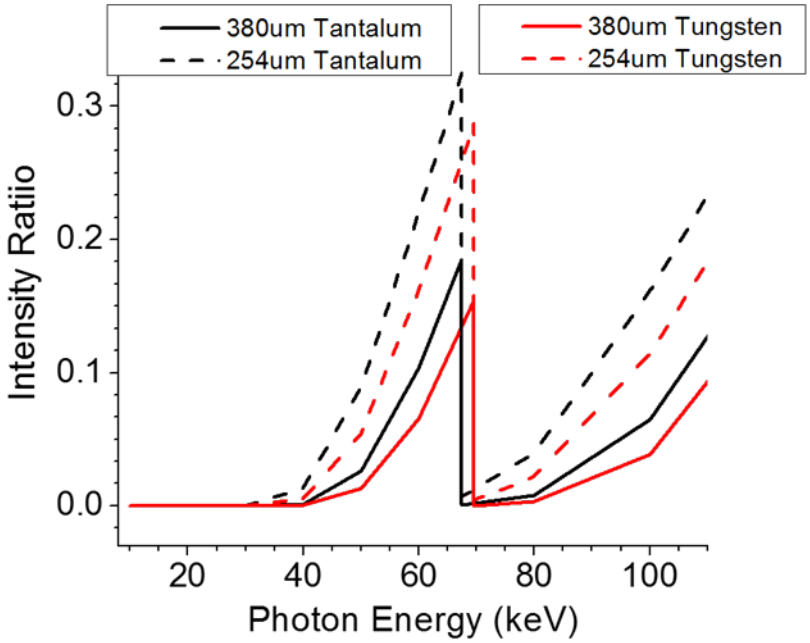

Fig. 9 X-ray photon attenuation of tungsten and tantalum sheets of 380- and 245-µm thicknesses

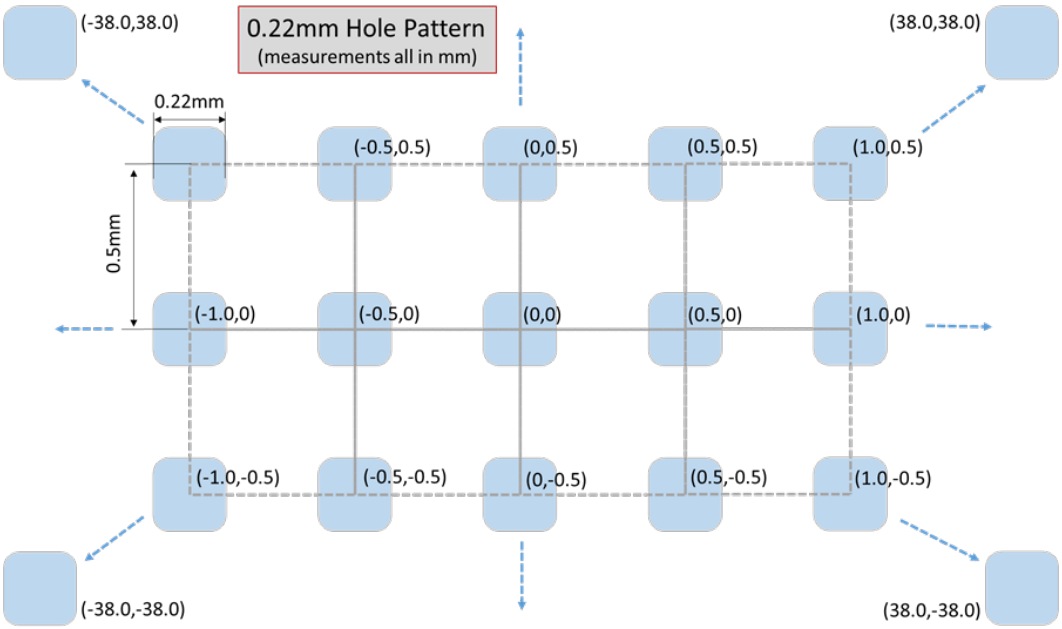

Fig. 10 Proposed shadow mask design for 0.38-mm-thick tungsten sheet for X-ray image detanglement with 0.5-mm resolution

4. Conclusion

A new capability was conceived and developed to capture multiple flash X-rays on a single film or phosphor screen and digitally detangle the resulting image into separate images for each individual flash. The geometric concept, computer algorithm, and experimental proof of principle were successfully completed using 4 flash X-rays with low-resolution copper masks. Extending the method for higher resolution masks has been outlined and a method of manufacture determined. This concept can be adapted to any experimental facility that currently has flash X-ray capability and will enable multiple flash X-rays during dynamic events without any flash-to-flash overlap in the images.

5. References

1. Abramson A. The history of television, 1942 to 2000. Jefferson (NC): McFarland & Co.; 2003.

2. Gilmore CP. Color TV: Is it finally worth the money? Popular Science. 1963 Aug;178:80–83.

3. Cazamias JU. Overlap areas of a square box on a square mesh. Aberdeen Proving Ground (MD): Army Research Laboratory (US); 2017 Apr. Report No.: ARL-TN-0818.

4. Hubbell JH, Seltzer SM. Tables of X-ray mass attenuation coefficients and mass energy-absorption coefficients from 1 keV to 20 MeV for elements Z = 1 to 92 and 48 additional substances of dosimetric interest. Gaithersburg (MD): National Institute of Standards and Technology; 2004 July. NISTIR 5632.

List of Symbols, Acronyms, and Abbreviations

2-D	2-dimensional
NIST	National Institute of Science and Technology
ORAD	original digital radiograph

1 (PDF)	DEFENSE TECHNICAL INFORMATION CTR DTIC OCA
2 (PDF)	DIR ARL RDRL CIO L IMAL HRA MAIL & RECORDS MGMT
1 (PDF)	GOVT PRINTG OFC A MALHOTRA
20 (PDF)	ARL RDRL WM E SCHOENFELD RDRL WML E P WEINACHT RDRL WML H B SCHUSTER RDRL WMP H LYON RDRL WMP A J CAZAMIAS S BILYK W UHLIG P BERNING M COPPINGER RDRL WMP B A SOKOLOW C HOPPEL RDRL WMP C R BECKER RDRL WMP D A BARD J RUNYEON M KEELE M ZELLNER R DONEY RDRL WMP E D HORNBAKER P SWOBODA S BARTUS